

Possible evidence for a variable fine structure constant from QSO absorption lines: systematic errors[★]

M. T. Murphy^{1†}, J. K. Webb¹, V. V. Flambaum¹, C. W. Churchill² and J. X. Prochaska³

¹*School of Physics, The University of New South Wales, UNSW Sydney NSW 2052, Australia*

²*Department of Astronomy & Astrophysics, Pennsylvania State University, University Park, PA, 16802, USA*

³*The Observatories of the Carnegie Institute of Washington, 813 Santa Barbara St. Pasadena, CA 91101*

Accepted —. Received —; in original form —

ABSTRACT

Comparison of quasar absorption spectra with laboratory spectra allow us to probe possible variations in the fundamental constants over cosmological time-scales. In a companion paper we present an analysis of Keck/HIRES spectra and report possible evidence suggesting that the fine structure constant, α , may have been smaller in the past: $\Delta\alpha/\alpha = (-0.72 \pm 0.18) \times 10^{-5}$ over the redshift range $0.5 < z < 3.5$. In this paper we describe a comprehensive investigation into possible systematic effects. Most of these do not significantly influence our results. When we correct for those which do produce a significant systematic effect in the data, the deviation of $\Delta\alpha/\alpha$ from zero becomes *more* significant. We are lead increasingly to the interpretation that α was slightly smaller in the past.

Key words: atomic data – line: profiles – instrumentation: spectrographs – methods: data analysis – techniques: spectroscopic – quasars: absorption lines

1 INTRODUCTION

The idea of varying fundamental constants is not a new one: Milne (1935, 1937) and Dirac (1937) independently suggested a varying Newton gravitational constant. More modern theories, such as superstring theory, naturally predict variations in fundamental coupling constants (e.g. Forgács & Horváth 1979; Marciano 1984; Barrow 1987; Li & Gott 1998), strongly motivating an experimental search. Several authors have demonstrated the idea (Varshalovich & Potekhin 1995 and references therein), first used by Bahcall, Sargent & Schmidt (1967), of using spectra of high redshift gas clouds seen in absorption against background quasars (QSOs) to constrain possible variation of the fine structure constant, $\alpha \equiv \frac{e^2}{\hbar c}$, over cosmological time-scales. This method is based on a comparison of the observed transition wavelengths of alkali doublets and recent applications of it have yielded constraints on $\Delta\alpha/\alpha \equiv (\alpha_z - \alpha_0)/\alpha_0 \sim 5 \times 10^{-5}$

where α_z and α_0 are the values of α at the absorption cloud redshift z and in the laboratory respectively (e.g. Cowie & Songaila 1995; Ivanchik, Potekhin & Varshalovich 1999; Varshalovich, Potekhin & Ivanchik 2000). Recently, we have increased the level of precision obtained with the alkali doublet method to $\Delta\alpha/\alpha = (-0.5 \pm 1.3) \times 10^{-5}$ using higher quality data (Murphy et al. 2000c).

However, a new method offering an order of magnitude improvement in precision was suggested by Dzuba, Flambaum & Webb (1999a,b) and was demonstrated by Webb et al. (1999, hereafter W99). The increase in precision derives from the fact that the relativistic corrections to the energy levels of different ions vary from species to species by up to an order of magnitude. A comparison of the observed Mg I, Mg II and Fe II transition wavelengths in 30 absorption systems allowed W99 to tentatively suggest that the mean value of $\Delta\alpha/\alpha = (-1.09 \pm 0.36) \times 10^{-5}$ over the redshift range $0.5 < z < 1.6$: the fine structure constant may have been smaller in the past.

The present work is the companion paper of Murphy et al. (2001a, hereafter M01a) in which we discuss our techniques in detail and present the results of recent work. We summarise the main points here. We obtained Keck/HIRES spectra of 28 QSOs and analysed 49 absorption systems lying along their lines of sight. These systems included those Mg II/Fe II systems considered in W99 and also a higher red-

[★] Data presented herein were obtained at the W.M. Keck Observatory, which is operated as a scientific partnership among the California Institute of Technology, the University of California and the National Aeronautics and Space Administration. The Observatory was made possible by the generous financial support of the W.M. Keck Foundation.

[†] E-mail: mim@phys.unsw.edu.au (MTM)

shift sample of damped Lyman- α systems (DLAs) containing absorption lines of ions such as Mg I, Mg II, Al II, Al III, Si II, Cr II, Fe II, Ni II and Zn II, so that our redshift range now covers $0.5 < z < 3.5$, corresponding to look-back times from 5 to 12 billion years ($H_0 = 68 \text{ km s}^{-1} \text{ Mpc}^{-1}$, $\Omega_M = 0.3$, $\Omega_\Lambda = 0.7$). Our absorption systems fell conveniently into two sub-samples: the Mg II/Fe II systems comprised the low redshift sample ($\bar{z} = 1.0$) and the DLAs comprised the high redshift sample ($\bar{z} = 2.1$). There were, however, 2 Mg II/Fe II absorbers within the high- z sample that lay at low redshift but we have included them in the high- z sample since the observations and data reduction for the two sub-samples were carried out independently by two different groups.

The analysis is based on the following equation for the wavenumber, ω_z , of a given transition at a redshift z ;

$$\omega_z = \omega_0 + q_1 x + q_2 y, \quad (1)$$

where ω_0 is the laboratory rest wavenumber of the transition, q_1 and q_2 are relativistic coefficients, $x \equiv (\alpha_z/\alpha_0)^2 - 1$ and $y \equiv (\alpha_z/\alpha_0)^4 - 1$. Note that the second and third terms on the right hand side only contribute if $\Delta\alpha/\alpha \neq 0$. The values of q_1 and q_2 have been calculated using many-body techniques in Dzuba et al. (1999a,b, 2001) and we tabulate those values relevant to our analysis in table 1 of M01a.

The values of ω_0 must be known to a high precision in order to place stringent constraints on $\Delta\alpha/\alpha$. A precision of $\Delta\alpha/\alpha \sim 10^{-5}$ corresponds to an uncertainty on $\omega_0 \sim 0.02 \text{ cm}^{-1}$ ($\sim 0.3 \text{ km s}^{-1}$)[‡]. This corresponds fairly well to the data quality since we can centroid an absorption feature to approximately one tenth of the HIRES resolution, $\sim 7 \text{ km s}^{-1}$. Such precision has not been previously achieved for most resonance transitions of ionized species and so measurements of ω_0 for all relevant species were carried out by several groups (Nave et al. 1991; Pickering, Thorne & Webb 1998; Pickering et al. 2000; Griesmann & Kling 2000) using laboratory Fourier transform spectrometers. We have summarised and tabulated these measurements in M01a.

Knowing all values of ω_0 , q_1 and q_2 , we then deconvolve each absorption system into individual Voigt components and perform a non-linear least squares χ^2 minimization to find the best-fitting value of $\Delta\alpha/\alpha$ at each absorption redshift. For the low- z sample we confirm the W99 result, our new results giving a weighted mean of $\Delta\alpha/\alpha = (-0.70 \pm 0.23) \times 10^{-5}$. For the new, high- z sample, we find a similar result: $\Delta\alpha/\alpha = (-0.76 \pm 0.28) \times 10^{-5}$. Both results independently suggest a smaller value of α in the past. Taking the sample as whole we find $\Delta\alpha/\alpha = (-0.72 \pm 0.18) \times 10^{-5}$, a 4σ result. These new results are also summarised in Webb et al. (2001, hereafter W01).

Given the potential importance of such a result for fundamental physics, a thorough investigation of possible systematic problems in the data or in the analysis is essential,

[‡] We can see this as follows. We can ignore the term in q_2 since these coefficients are typically an order of magnitude smaller than the q_1 coefficients. Consider two transitions, one with a low atomic mass, the other a high atomic mass. Typically, the difference between the q_1 coefficients for a light species (e.g. Mg II) and a heavy species (e.g. Fe II) is $\sim 1000 \text{ cm}^{-1}$. Equation 1, applied to these two transitions, then shows that a precision of ω_0 of $\sim 0.02 \text{ cm}^{-1}$ is required in order to detect a variation of $\Delta\alpha/\alpha \sim 10^{-5}$.

and this is the purpose of the present paper. In Section 2 we list all effects that one might consider as being able to mimic a systematically non-zero $\Delta\alpha/\alpha$. We are able to exclude many of them with general arguments. Sections 3–7 are then given over to a more detailed analysis of five specific effects: wavelength mis-calibration, ionic line blending, atmospheric dispersion effects, differential isotopic saturation and possible isotopic variation. Section 8 describes another test which is sensitive to a simple monotonic wavelength distortion, specifically for the high- z sample. We make our conclusions in Section 9.

2 SUMMARY OF POTENTIAL SYSTEMATIC ERRORS

In M01a and W01 we found that values of $\Delta\alpha/\alpha$ were systematically negative and that this trend was evident in two different samples of data occupying different redshift regimes. We note that the low- z sample is more susceptible to systematic errors than the high- z sample. The Mg II lines act as anchors against which the larger Fe II shifts can be measured. All of the Fe II lines have similar magnitude shifts in the same direction (i.e. q_1 is large and positive in all cases). Furthermore, all the Fe II lines lie to the blue of the Mg II doublet. If some systematic error in the wavelength scale is present, which effectively *compresses* the spectrum, this would mimic a negative shift in the mean value of $\Delta\alpha/\alpha$ (if it were not degenerate with redshift). The high- z sample is far more complex in this regard since it contains ions not only with positive coefficients, but also with negative q_1 coefficients (i.e. all Cr II lines and Ni II $\lambda 1741$ and $\lambda 1751$). Also, the shifts for the various ions are of various magnitudes making it more complicated to predict the effect of a systematic error on our measured values of $\Delta\alpha/\alpha$.

2.1 Laboratory wavelength errors

Errors in the values of ω_0 will lead directly to errors in any single determination of $\Delta\alpha/\alpha$. If, for example, the laboratory wavelengths of the Mg II lines were all shifted to the blue or red then this would systematically bias the values of $\Delta\alpha/\alpha$ for the low- z sample. In M01a we summarise the measurements of all values of ω_0 . Most measurements were repeated independently and good agreement was obtained in those cases. A typical measurement accuracy from these laboratory measurements ω_0 of is $\sim 2 \times 10^{-3} \text{ cm}^{-1}$, which could only introduce a maximum error in $\Delta\alpha/\alpha$ around an order of magnitude below the observed deviation from zero. In practice, since we use several transitions (particularly for the high- z sample), any associated errors are likely to be smaller. We therefore consider it unlikely that the systematic shift in $\Delta\alpha/\alpha$ is due to errors in the values of ω_0 .

As also noted in M01a, some laboratory spectra were calibrated with the Ar II lines of Norlén (1973) while others were calibrated with those of Whaling et al. (1995). The Whaling wavenumbers are systematically larger than those of Norlén such that $\Delta\omega = 7 \times 10^{-8}\omega$. To deal with this discrepancy we have re-scaled those wavenumbers which had been calibrated using the Whaling scale (Al II, Al III, Si II) to the Norlén scale. We stress that the difference between the Norlén and Whaling wavenumbers is a *scaling only*, and

not a distortion. Therefore, is it not possible to introduce an apparent deviation in $\Delta\alpha/\alpha$ from zero, since small zero-point offsets in the wavelength scale are degenerate with redshift.

2.2 Heliocentric velocity variation

During a one hour exposure, representative of the quasar integrations for the sample we have used, the heliocentric velocity may change by as much as $\sim 0.1 \text{ km s}^{-1}$. This will act to smear any spectral feature: the instantaneous spectrum is convolved with a top hat function in velocity space. However, since we fit a redshift parameter to the spectrum when determining $\Delta\alpha/\alpha$ then a velocity space smearing is completely absorbed into the redshift parameter. Heliocentric smearing will have no effect on measurements of $\Delta\alpha/\alpha$.

2.3 Differential isotopic saturation

The ions used in our analysis, with the exception of those of Al, have naturally occurring isotopes. Thus, each absorption line will be a composite of absorption lines from all the isotopes of a given species. In all cases other than Mg and Si, the laboratory wavenumbers we have used correspond to *composite* values. The composite wavenumbers will only strictly be applicable in the optically thin regime (linear part of the curve of growth). As the column density increases, the strongest isotopic component begins to saturate and the line centroid will shift according to the natural abundances (cf. Section 2.4) of the other isotopes.

The mass isotopic shift, being the dominant splitting mechanism for light atoms, is proportional to ω_0/m^2 for m the atomic mass. The wavelength separation between the isotopes is therefore largest for the lighter (low q_1) ions. Isotopic separations have been measured for the Mg I $\lambda 2853$ transition by Hallstadius (1979), for Mg II $\lambda 2796$ by Drullinger et al. (1980) and the isotopic structure of all Mg lines is presented in Pickering et al. (1998). However, similar measurements do not exist for the other transitions of interest. For Si we used estimates of the isotopic wavenumbers based on a scaling from the basic Mg structure by the mass shift. For all other species, measured (composite) wavenumbers were used. See M01a for full details.

We discuss and quantify this effect in Section 6.

2.4 Isotopic abundance variation

In the above we have assumed that the isotopic abundances in the absorption systems are equal to terrestrial values (Table 3). However, if the isotopic abundances at high redshift are significantly different then this may lead to apparent shifts in the absorption line centroids and this would cause a systematic error in $\Delta\alpha/\alpha$. Again, the most susceptible transitions are those of Mg and Si since (i) these ions will have the largest isotopic separations (i.e. m is low) and (ii) transitions in these atoms are prominent in our data. If, for the low- z sample, the ^{25}Mg and ^{26}Mg abundances were zero, we would incorrectly infer a more positive $\Delta\alpha/\alpha$ by assuming terrestrial isotopic abundances. In the simple case of finding $\Delta\alpha/\alpha$ from Mg II $\lambda 2796$ and Fe II $\lambda 2344$, we would

expect to find $\Delta\alpha/\alpha \approx 0.6 \times 10^{-5}$ in the absence of any real variation in α .

We consider this possibility in detail in Section 7

2.5 Hyperfine structure effects

Hyperfine splitting of energy levels occurs in species with odd proton or neutron numbers. Different hyperfine components will have different transition probabilities but the composite wavelength of a line will be unchanged by the splitting (i.e. the centre of gravity of the hyperfine components is constant with increased splitting). However, a similar differential saturation effect will occur for the hyperfine components as discussed in Section 2.3 for the isotopic components.

The worst case here is that of ^{27}Al – the only stable isotope of Al – since it has an odd proton number and a very large magnetic moment. In the laboratory experiments of Griesmann & Kling (2000), the hyperfine structure of the Al III doublet was clearly resolved and can be seen to be quite prominent. However, as noted in M01a, we only include Al III lines in the analysis of 6 absorption systems of our high- z sample and in these cases we see very little or no saturation. The effect of removing the individual Al III transitions from those systems on $\Delta\alpha/\alpha$ can be seen in Fig. 4. In the case of Al II $\lambda 1670$, both the ground and excited state have zero spin and the p -wave hyperfine splitting in the excited state is very small (cf. ^{25}Mg in Pickering et al. 1998). Thus, we do not expect any Al hyperfine saturation effects on $\Delta\alpha/\alpha$.

All other dominant isotopes in our analysis have even proton numbers and where odd isotopes occur these have very low abundances (see Table 3). The ^{25}Mg hyperfine structure has already been taken into account in our analysis but the hyperfine separations are so small that neglecting it would make no difference to $\Delta\alpha/\alpha$ even upon saturation. The odd isotopes of Si, Cr, Fe, Zn and Ni have very low abundances. Also, Si, Cr, Fe and Ni will have very small hyperfine splitting due either to low magnetic moments or to the nature of the ground and excited state wavefunctions.

We therefore expect that differential hyperfine structure saturation has not effected $\Delta\alpha/\alpha$ in our analysis. An unlikely interpretation, given the above, is cosmological evolution of the hyperfine structure constants but very large relative variations would be required.

Another possibility is that the populations of the two hyperfine levels of Al III are not equal in the absorption clouds. Since the gas clouds have very low density, the equilibrium between the two hyperfine levels will be maintained predominantly by interaction with cosmic microwave background (CMB) photons. For the Al III $\lambda 1862$ transition, this implies a lower limit on the relative populations of the two levels of $\exp(-\Delta\omega/k_{\text{B}}T_{\text{CMB}}) \approx 0.9$, leading to a shift in the line centroid of $\sim 0.01 \text{ cm}^{-1}$ ($\sim 5 \times 10^{-4} \text{ \AA}$). This is a potential problem for the 6 systems in which we fit Al III lines. We do not consider this effect in detail but we note that Fig. 4 in Section 4.2 shows that potential lack of thermal equilibrium has no significant effect on $\Delta\alpha/\alpha$.

2.6 Magnetic fields

Shifting of ionic energy levels due to large magnetic fields may also be a possibility. If very large scale magnetic fields exist in the intergalactic medium and quasar light is polarized, then this could result in correlated values of $\Delta\alpha/\alpha$ in neighbouring regions of the universe. However, the QSOs studied in M01a and W01 cover a large region of the sky. Furthermore, even in Abell clusters, intra-cluster magnetic field strengths are typically $\sim \mu\text{G}$ (e.g. Feretti et al. 1999), roughly 9 orders of magnitude below the strength required to cause substantial effects. We consider this possibility to be very unlikely.

2.7 Kinematic effects

An assumption in the analysis of M01a and W01 is that the absorption velocity structure is the same in different species. Of course, if there were some non-zero velocity between, say, the Mg II and Fe II components of a given cloud then we would incorrectly determine $\Delta\alpha/\alpha$. However, it is difficult to imagine a mechanism by which the Mg II is systematically blue or redshifted with respect to the Fe II when averaged over a large sample of absorption systems. Suppose for example we have an asymmetric, expanding (or contracting), rotating cloud in which all the Fe II and Mg II lie at different ‘radii’. Any large sample of sight lines through such a cloud would yield an average value of $\Delta\alpha/\alpha = 0$. Furthermore, if this was a major effect then the observed scatter in the $\Delta\alpha/\alpha$ points would be greater than expected on the basis of our $\Delta\alpha/\alpha$ error estimates, and in M01a we showed this not to be the case. No matter how contrived the velocity structure and ionic segregation, when averaging over a large number of values of $\Delta\alpha/\alpha$, it is not feasible to generate a systematic offset from zero.

2.8 Wavelength mis-calibration

There may be inaccuracies in the wavelength calibration software used to reduce the spectra. Also, human error cannot be ruled out. W99 stated that a drift in the wavelength calibration drift by an amount corresponding to roughly ~ 2.5 times the mean wavelength-pixel residuals over the range of the CCD could result in a significant error in the low- z results. A considerably more complicated form of the mis-calibration would be required to produce a systematic error in the high- z results.

The wavelength calibration of the QSO CCD images is done by comparison with Thorium–Argon (ThAr) lamp exposures taken before and after the QSO frames. We consider errors in the laboratory wavelengths of the selected ThAr lines to be negligible as their relative values are known to much greater precision than our values of ω_0 (Palmer & Engleman Jr. 1983). However, ThAr line mis-identifications may lead to serious mis-calibration of the wavelength scale over large wavelength regions. Such mis-identifications can also be applied to the rest of the spectra taken over the same series of observations (i.e. applied to the spectra of many QSOs). Thus, *a priori*, we cannot rule out the possibility that the wavelength scale has been set improperly in this process and that a systematic shift in α has not been mimicked. Such a potential effect needs careful investigation.

In Section 3 we discuss and quantify this effect for our data set.

2.9 Air–vacuum wavelength conversion

Most ThAr line lists are presented as air wavelengths. The usual data reduction procedure is to carry out the wavelength calibration fits to the data using air wavelengths and then convert the calibrated spectrum to vacuum wavelengths. For example, IRAF[§] uses air wavelengths for a selection of lines from the Thorium spectral atlas of Palmer & Engleman Jr. (1983) and from the Argon lines of Norlén (1973). The same list is used in MAKEE – the HIRES data reduction package written by T. Barlow. MAKEE was used to calibrate 12 of our high- z sample and the remainder were calibrated within IRAF. The latter were actually calibrated with a set of vacuum wavelengths, λ_{vac} , that IRAF states is derived from the air wavelengths, λ_{air} , by using the Edlén (1966) formula for the refractive index, n ,

$$10^8 [n(\lambda_{\text{vac}}) - 1] = 8342.13 + \frac{2406030}{(130 - \sigma^2)} + \frac{15997}{(38.9 - \sigma^2)} \quad (2)$$

at 15°C and atmospheric pressure. Instead of using $\sigma \equiv 10^4/\lambda_{\text{vac}}$, IRAF makes the approximation, $\sigma \approx 10^4/\lambda_{\text{air}}$. MAKEE converts the final air wavelength calibrated QSO frames to vacuum using the Cauchy dispersion formula (Weast 1979),

$$10^7 [n(\lambda_{\text{air}}) - 1] = 2726.43 + \frac{12.288}{10^{-8}\lambda_{\text{air}}^2} + \frac{0.3555}{10^{-16}\lambda_{\text{air}}^4} \quad (3)$$

at 15°C and atmospheric pressure. λ_{vac} and λ_{air} are both measured in Ångstroms in the above equations. This difference begs the question, what is the absolute and relative accuracy of these conversion formula?

First let us refine this question. The measurements reported by Palmer & Engleman Jr. and Norlén were all carried out in vacuum. The air wavelengths they quote are calculated using the Edlén formula. Thus, IRAF and MAKEE will only produce ‘correct’ vacuum wavelength scales if they invert the Edlén formula to calculate the refractive index. As stated above, this is not the case. Therefore, to re-state the above question, what error does the IRAF and MAKEE air–vacuum wavelength conversion introduce into the resulting QSO wavelength scale? To illustrate the answer to this we plot the various conversion formulae commonly used in the literature, including those discussed above, in Fig. 1. We have also included the original Edlén (1953) formula[¶] for comparative purposes. Peck & Reeder (1972) published a fit to revised refractive index data, proposing a 4-parameter formula:

$$10^8 [n(\lambda_{\text{vac}}) - 1] = \frac{5791817}{(238.0185 - \sigma^2)} + \frac{167909}{(57.362 - \sigma^2)} \quad (4)$$

[§] IRAF is distributed by the National Optical Astronomy Observatories, which are operated by the Association of Universities for Research in Astronomy, Inc., under cooperative agreement with the National Science Foundation.

[¶] The Edlén (1953) formula is of the same form as the 1966 formula (equation 2) but has slightly different parameters: 6432.8, 2949810, 146, 25540 and 41 in order from left to right, numerator to denominator.

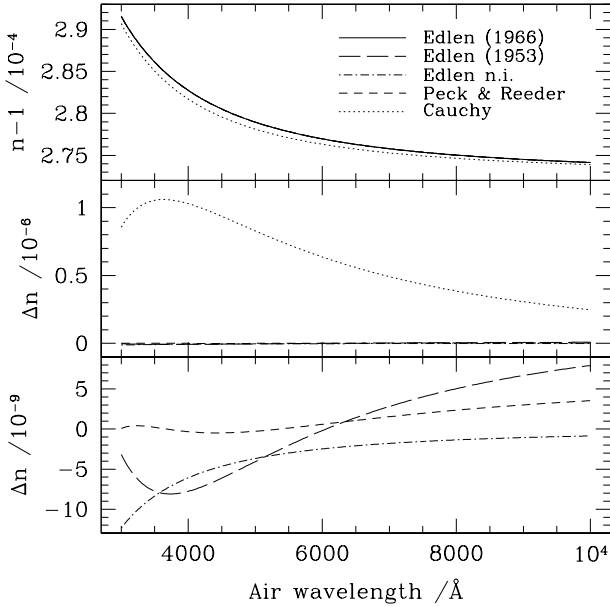


Figure 1. Comparison of the various air dispersion formulas used in the literature (all for 15°C and atmospheric pressure). We use the Edlén (1966) formula as our reference since the atlases of Palmer & Engleman Jr. (1983) and Norlén (1973) use this to convert their vacuum wavelengths to air wavelengths. The top panel shows the dispersion for the Edlén (1966) and Edlén (1953) formulas together with that of Peck & Reeder (1972) and the Cauchy formula (Weast 1979). We also plot the approximation made within IRAF where the Edlén formula has not been inverted to convert air wavelengths to vacuum (denoted “Edlén n.i.”). The middle and lower panels show the difference between the Edlén (1966) refractive index, n_E , and that derived from the other formulae, n_X : $\Delta n \equiv n_E - n_X$.

at 15°C and atmospheric pressure with $\sigma \equiv 10^4/\lambda_{\text{vac}}$ (again, λ_{vac} is in Ångströms).

From Fig. 1 we see that the Cauchy formula seriously deviates from the other formulas. Furthermore, the difference between the Edlén and Cauchy dispersions is strongly wavelength dependent. Thus, spectra calibrated with MAKEE may have systematically non-zero values of $\Delta\alpha/\alpha$ due to this distortion. As we stated in M01a, we have corrected the 12 effected spectra in our (high- z) sample by converting the wavelength scale back to air wavelengths using the (inverted) Cauchy formula and then back to vacuum using the (inverted) Edlén formula. From Fig. 1 we can also see that there is only a small distortion to the wavelength scale introduced due to the approximation made within IRAF. This difference is below our level of precision.

2.10 Temperature changes during observations

The refractive index of air within the spectrograph depends on temperature (and also on pressure but this is a smaller effect). If a QSO spectrum is calibrated with only a single ThAr exposure taken at a different spectrograph temperature, we expect a systematic mis-calibration of the QSO frame’s wavelength scale. Consider a QSO frame taken at 15°C which is calibrated with a ThAr exposure taken at 0°C

and similar pressure. Any wavelength separation in the QSO exposure will be overestimated. For example, the difference between the wavelength separations of vacuum $\lambda 4000$ and $\lambda 7000$ Å at 15°C and 0°C is 43×10^{-3} Å (using the tables in Weast 1979). A comparison with values of $\Delta\lambda$ in table 1 of M01a shows that this would result in a significantly positive $\Delta\alpha/\alpha$ for the low- z sample, the situation not being so clear for the high- z sample.

Note that the above effect can only mimic a systematically non-zero $\Delta\alpha/\alpha$ if the spectrograph temperature is systematically higher or lower for the ThAr frames compared with the QSO frames. This is possible if the ThAr exposures were always taken before or after the QSO frames and the temperature evolves monotonically throughout the night. However, the effect is greatly reduced if ThAr exposures are taken near the time of the QSO observations. This was the case in our observations. We have used image header information to calculate the QSO–ThAr temperature difference, $\Delta T \equiv \langle T_{\text{QSO}} \rangle - \langle T_{\text{ThAr}} \rangle$, inside HIRES for both the low and high- z samples. Here the average of T_{QSO} and T_{ThAr} is taken over all exposures for each object. We find mean values of $\Delta T = 0.04 \pm 0.02$ K and $\Delta T = 0.2 \pm 0.1$ K for the low and high- z samples respectively. Taking into account that, on average, rest-frame separations between transitions are $\lesssim 300$ Å then we can see that temperature variations could not have mimicked any significant shift in $\Delta\alpha/\alpha$ in either sample.

2.11 Line blending

The errors in $\Delta\alpha/\alpha$ presented in M01a and W01 take into account errors from signal-to-noise and spectral resolution considerations and the velocity structure of the profile fits. The errors are also reduced when more lines are fitted simultaneously. However, we have assumed that we have deconvolved each absorption system into the correct number of velocity components. There may have been weak, interloping, unresolved lines which, if the interloping species were in the same absorption cloud, could have produced a shift in the fitted line wavelengths of all velocity components of one or more transitions.

We distinguish between *random* blends and *systematic* blends. *Random* blends may occur if many absorption clouds at different redshifts intersect the line of sight to a single QSO. A *systematic* blend will occur when two species are in the same cloud and have absorption lines with similar rest-wavelengths. Such an effect could mimic a systematic shift in α .

The importance of such an effect diminishes as the number of transitions used in each fit is increased. Therefore, the effect, if present, would be expected to be smaller in our high- z sample.

In Section 4 we describe the results of a detailed search for atomic (and not molecular) interlopers for all transitions of interest, and place constraints on their strengths and positions.

2.12 Atmospheric dispersion effects

As noted in M01a, all of the low- z sample and many of the high redshift sample of QSOs were observed before 1996 August at which time an image rotator was fitted to HIRES.

Objects observed prior to August 1996 were therefore not observed with the slit length (spatial direction) perpendicular to the horizon. Atmospheric dispersion leads to a stretching of the target spectrum relative to the calibration spectrum.

An additional consequence is the potential wavelength-dependent truncation of the QSO seeing profile on the slit jaw edges. This can introduce a wavelength dependent asymmetry in the point-spread function (PSF).

Together, these effects can conspire to mimic a non-zero $\Delta\alpha/\alpha$. We provide detailed calculations for these effects in Section 5 and show that they will tend to produce an apparent *positive* $\Delta\alpha/\alpha$, and so cannot mimic our results.

2.13 Instrumental profile variations

If the instrumental profile (IP) of HIRES shows significant *intrinsic* asymmetries then we expect absorption line centroids to be incorrectly estimated. If the asymmetry varies with wavelength, this could mimic a non-zero $\Delta\alpha/\alpha$. Valenti, Butler & Marcy (1995) have determined the HIRES IP for several positions along a single order and they find that the IP is indeed asymmetric and that the asymmetry varies slightly along the echelle order. Valenti et al. (1995), do not quantify the asymmetry variation across orders although it is likely to be comparable to the variation along the orders.

As a by-product of the detailed investigation into possible wavelength calibration errors, we find that this effect is negligible (see Section 3 for details).

We have therefore eliminated, with some reliability, potential systematic errors due to: laboratory wavelength errors, heliocentric velocity variation, hyperfine structure effects, magnetic fields, kinematic effects, air–vacuum wavelength conversion errors and temperature changes during observations.

In the following sections we investigate in considerable detail the remaining effects: wavelength mis-calibration (and instrumental profile variations), line blending, atmospheric dispersion effects, differential isotopic saturation and isotopic abundance variation. We also consider a simple test for any simple but unidentified systematic errors for the high- z sample in Section 8.

3 DETAILED ANALYSIS: WAVELENGTH CALIBRATION ERRORS

In this section, we investigate the possibility that wavelength calibration errors could have lead to an apparent non-zero $\Delta\alpha/\alpha$. To quantify this directly, we analyse sets of ThAr emission lines in the calibration lamp spectra in the same way as each set of QSO absorption lines has been analysed. If no calibration error is present then we expect that $(\Delta\alpha/\alpha)_{\text{ThAr}} = 0$ for all clouds (i.e. for all z).

3.1 Method

For each QSO spectrum, we selected $\sim 15 \text{ \AA}$ sections of ThAr spectra at wavelengths corresponding to the observed absorption lines in the QSO spectra. Each ThAr $\sim 15 \text{ \AA}$ section contains several (typically up to ~ 10) lines. Error ar-

rays were generated assuming Poisson counting statistics. We fitted continua to these ThAr sections, dividing the raw spectra by the continua to obtain normalized spectra.

The main steps in the procedure are then as follows. We select several independent sets^{||} of ThAr lines. Each set of ThAr lines therefore corresponds to, and has been selected in an analogous way to, one QSO absorption system.

In order to obtain the best estimate of any wavelength calibration errors, the average $(\Delta\alpha/\alpha)_{\text{ThAr}}$ is determined for each ThAr set (typically 3–7 sets for each QSO absorption system). The process of defining sets in this way also provides a direct additional estimate of the errors on $(\Delta\alpha/\alpha)_{\text{ThAr}}$.

To fit the ThAr spectra, a modified version of VPFIT was used (to fit Gaussian profiles, see M01a), adopting ThAr laboratory wavelengths from Palmer & Engleman Jr. (1983) for values of ω_0 in equation 1. The q_1 and q_2 coefficients for the QSO absorption lines are applied to the corresponding ThAr lines. That is, we treat the set of ThAr lines as if they were the QSO lines. The free parameters involved in each fit were line width (assumed the same for all ThAr lines in a given set, although the results were insensitive to this assumption), ‘redshift’ (numerically close to zero) and peak intensity.

3.2 Results and Discussion

We applied the above method to each available ThAr spectrum corresponding to each QSO absorption cloud considered and the results are illustrated in Fig. 2. Our first observation is that the scatter in these results is an order of magnitude less than that of the QSO absorption results themselves. This clearly demonstrates that wavelength mis-calibration of the CCD has not mimicked a shift in α to any significant degree. The results above also show that the data quality permit a precision of $\Delta\alpha/\alpha \sim 10^{-7}$.

Secondly, many points in Fig. 2 deviate significantly from zero. There are three possible reasons for this: weak blended emission lines, ThAr line mis-identifications, and errors in the ThAr laboratory wavelengths. Inspecting the ThAr spectra does indeed reveal typically ~ 20 easily identifiable, but very weak, lines per 15 \AA and we would expect this to add to the scatter in the final results for $(\Delta\alpha/\alpha)_{\text{ThAr}}$. Furthermore, this effect would not produce correlated deviations in $(\Delta\alpha/\alpha)_{\text{ThAr}}$, as observed. Consistent with this interpretation, we found that the value of χ^2 per degree of freedom for a fit to a given set of ThAr lines was $\gg 1$. Note that if ThAr line mis-identifications had occurred, one may expect systematically correlated deviations. Finally, we do not expect any significant errors in the ThAr laboratory wavelengths (as discussed in Section 2.8).

On inspection of some of the ThAr spectra, we noted that some ThAr lines towards the blue end of the spectrum were slightly asymmetric. This may indicate a degradation in the polynomial fits near the edges of the fitting regions. There may also be intrinsic asymmetries in the IP (Section 2.13). If such asymmetry variations exist then they should also apply to the QSO spectra. However, the results in Fig. 2

^{||} Each set of ThAr lines never included any of the ThAr lines from any other set.

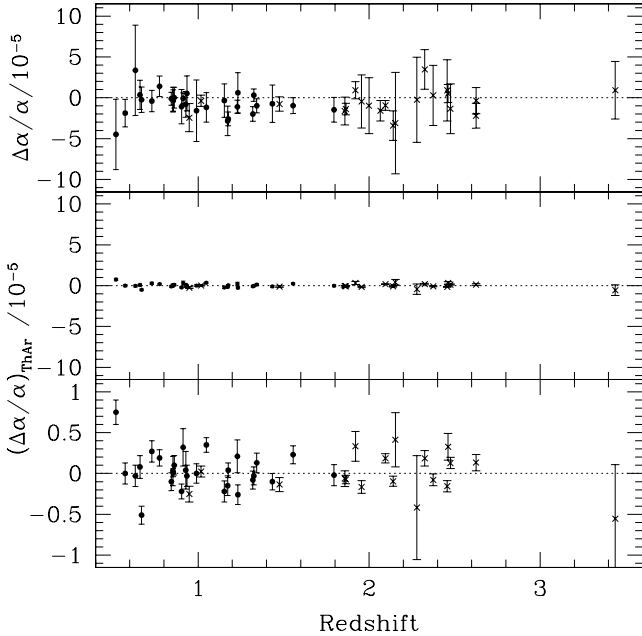


Figure 2. The top panel shows the results of M01a and W01. The middle panel compares the ThAr calibration error on the same scale. The lower panel gives an expanded view of the ThAr results. The weighted mean of the ThAr sample is $(0.0 \pm 1.4) \times 10^{-7}$. ThAr data were not available for five of the absorption systems. Clearly, this does not effect our conclusions.

show that such variations do not produce a systematic effect in $\Delta\alpha/\alpha$ at any detectable level.

We therefore conclude this section by stating that the results in Fig. 2 show unambiguously that wavelength calibration errors and variations in IP asymmetries are not responsible for the observed shifts in α in the QSO absorption line results.

4 DETAILED ANALYSIS: SYSTEMATIC LINE BLENDING WITH UNKNOWN SPECIES

In this section we suppose there is an unidentified transition, arising from some species in the same gas cloud as is being studied. We further assume that this interloping transition is not strong enough and/or sufficiently displaced from one of the lines in the analysis, to be detected directly. We describe two approaches to explore this: in Section 4.1 we attempt to identify candidate blending species and in Section 4.2 we describe the results of a test where we remove one transition or one species at a time to investigate the impact on $\Delta\alpha/\alpha$.

4.1 Search for potential interlopers

There are two main parameters which will determine whether or not any particular interloper can give rise to a significant effect in terms of $\Delta\alpha/\alpha$: column density and the position in wavelength with respect to the ‘host’ line of interest. In order to search for a potential interloper, we explore the range in parameter space through numerical simulation, generating trial interlopers, blended with a single stronger

‘host’ line, and examining the resulting shift in the combined centroid in terms of $\Delta\alpha/\alpha$. Having established the allowed characteristics of a potential interloper, we use photoionization equilibrium models to search for candidate atomic species. We ignore molecular species.

4.1.1 Characteristics of a candidate interloper

We restrict the following discussion to blending with Mg II $\lambda 2796$, since $\Delta\alpha/\alpha$ is particularly sensitive to blending with this anchor line in the low- z sample. We later generalize our discussion to include blending with all other relevant transitions.

Consider an interloper – a spectral line of a blending species X – which is separated from the fitted line centroid wavelength, λ_0 , by $-\Delta\lambda$ ($\Delta\lambda > 0$) in the frame of the cloud. Let the separation between the actual Mg II $\lambda 2796$ wavelength and the fitted line position be $d\lambda$ (i.e. $d\lambda > 0$) in the frame of the cloud. That is, the line is fit as a single component, despite the presence of the interloper. The interloper has a column density $N(X)$. However, as the species X is not known *a priori*, we may only determine the quantity $N(X)f_X$ where f_X is the oscillator strength of the interloping transition.

We generated a synthetic optically thin Mg II $\lambda 2796$ line and matched this against a composite Mg II $\lambda 2796$ profile which included an additional weak blended component, representing our candidate interloper. The model was fitted to the ‘data’ using VPFIT. The synthetic spectrum was generated using a column density of $4 \times 10^{12} \text{ cm}^{-2}$ and a b -parameter of 5.0 kms^{-1} as these were representative values for the Mg II lines in M01a and W01 (Churchill 1997).

We restricted the range of b -parameters for the interloper using the following physical considerations. If we consider all lines to be thermally broadened then the b -parameter varies inversely as the square root of the atomic mass. Any species lighter than Mg will have a larger b -parameter. Since we are considering X to have transitions in the ultraviolet, we may assume that it probably has a mass greater than or comparable to that of Mg. We therefore place an upper limit of $b(X) < 6.0 \text{ kms}^{-1}$. Also, we did not consider any species with atomic number greater than ~ 100 and so we adopted a lower limit of $b(X) > 0.5 \text{ kms}^{-1}$.

By comparing sets of model and synthetic blended lines in this way, we can constrain the range of possible values of $d\lambda$, given some apparent $\Delta\alpha/\alpha$.

We present the results of the simulation in Fig. 3 where we define $\Gamma_{X,\text{Mg II}} \equiv \log_{10}[N(X)/N(\text{Mg II})]$ and $F_X \equiv \log_{10} f_X$. The ripples on the three surface reflect errors ($\lesssim 0.1$ dex in $\Gamma_{X,\text{Mg II}}$) introduced due to the restrictive upper limit placed on $b(X)$.

Using Fig. 3, we can now specify a certain value of $\Delta\alpha/\alpha$ (i.e. we specify $d\lambda$) and an interloping transition of a species X (i.e. we specify $\Delta\lambda$) and find the lower bound on the column density which that species must have in order to have caused the said shift in $\Delta\alpha/\alpha$. For example, if we are concerned with $\Delta\alpha/\alpha \sim 10^{-5}$ then $d\lambda \sim 50 \times 10^{-4} \text{ \AA}$ and the section of Fig. 3 with $d\lambda \lesssim 50 \times 10^{-4} \text{ \AA}$ contains information which restricts the candidate interlopers.

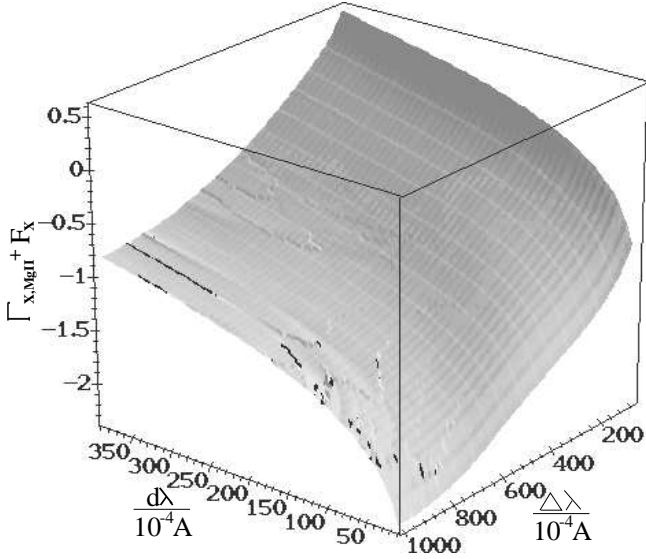


Figure 3. Three space of results from the blending simulation. $d\lambda$ directly corresponds to a value of $\Delta\alpha/\alpha$ if blending is responsible for all observed shifts in figure 3 of M01a. The figure is shaded according to values of $\Gamma_{X,\text{MgII}}$. Ripples on the surface reflect errors due to the restrictive upper bound on $b(X)$. The ‘lighting’ of the figure has been adjusted to maximize their visibility and the main errors have been highlighted in black.

4.1.2 Photoionization Modeling

Given a species, X , what is an upper limit on the column density in any given cloud? To answer this, we modelled the absorption clouds with a grid of CLOUDY models (Ferland 1993). CLOUDY estimates the photoionization conditions in absorption clouds by assuming that the cloud can be approximated as a series of zones, in a plane parallel geometry, illuminated by UV radiation from one direction. The fact that we are trying to model a (presumably) spherical cloud with UV flux incident from all sides is expected to introduce abundance errors of order a factor of 2 (Ferland 1993).

Photoionization equilibrium is characterized by (a) the shape and intensity of the UV spectrum, (b) the number density of hydrogen atoms in the cloud, n_{H} , (c) the size of the cloud, which we assume is the same for all species (the size can be found by specifying n_{H} and $N(\text{H I})$, the neutral hydrogen column density) and (d) the metallicity, Z , of the cloud. It is also useful to define the ionization parameter as $U \equiv n_{\gamma}/n_{\text{H}}$, where n_{γ} is the number density of ionizing photons incident on the cloud. Here we follow the work in Bergeron & Stasińska (1986), Bechtold et al. (1987), Steidel & Sargent (1989) and Bergeron et al. (1994) and choose a power law spectrum, $f_{\nu} \propto \nu^{-3/2}$, for f_{ν} the incident flux at frequency ν . The low and high energy extremes are given by $f_{\nu} \propto \nu^{5/2}$ (for $\lambda_{\nu} > 10 \mu\text{m}$) and $f_{\nu} \propto \nu^{-2}$ (for $E_{\nu} > 50 \text{keV}$).

All the above parameters (U , n_{H} , $N(\text{H I})$ and Z), vary from cloud to cloud and are poorly known quantities. We therefore use a grid of cloudy models to find an upper limit on the column density of a given ionic species using ranges in these parameters as follows. For U we adopt the range $-4 < \log_{10} U < -3$ in line with the measured range of parameters for those clouds studied in M01a and W01 (Churchill 1997).

Similarly, for $N(\text{H I})$ we use $17.0 < \log_{10} N(\text{H I}) < 19.0$. For Z we adopt a conservative range, $-2 < Z < 0$ (following Morris et al. 1986; Bergeron & Stasińska 1986; Bechtold et al. 1987; Steidel & Sargent 1989; Bergeron et al. 1994; Churchill 1997). The range of parameters we explore here are characteristic of the low redshift sample. For a related discussion of DLAs, see Prochaska (1999) and Prochaska & Wolfe (2000).

n_{H} is the most difficult parameter to constrain. To obtain an estimate of the lower bound, one may use the method, first suggested by Bahcall (1967), whereby one places an upper limit on n_{p} , the number density of protons in the cloud, using the equation,

$$\frac{N(\text{C II}^*)}{N(\text{C II})} = 3.9 \times 10^{-2} n_{\text{e}} \left(1 + 0.22 \frac{n_{\text{p}}}{n_{\text{e}}} \right). \quad (5)$$

Here, $N(\text{C II}^*)$ is the column density of C II which has been collisionally excited to the state C II*. n_{e} is the electron number density. We assume that $n_{\text{e}} \sim n_{\text{p}}$ and that $n_{\text{p}} \sim n_{\text{H}}$, and so, using $N(\text{C II}) = 4.6 \times 10^{14} \text{cm}^{-2}$ and $N(\text{C II}^*) < 10^{12} \text{cm}^{-2}$ from Songaila et al. (1994), we estimate that $\log_{10} n_{\text{H}} < -1.3$. Under these simple assumptions, this value is consistent with Morris et al. (1986) estimate, $\log_{10} n_{\text{H}} < 0.0$, and we adopt this as a conservative upper limit. A lower limit may be obtained by using upper limits on the cloud sizes. We used results from Bergeron & Stasińska (1986) to place a lower limit of $\log_{10} n_{\text{H}} > -3$ where we have used CLOUDY to estimate that $N(\text{H I}) \sim N(\text{H})/1000$. We compare our parameter range estimates above with those assumed in Lopez et al. (1999) and find that they are consistent after considering the differences between the assumed radiation field.

We present the results of the grid of CLOUDY models in Table 1 where we only give the value of $\Gamma_{X,\text{MgII}}^{\text{max}}$, the maximum value of $\Gamma_{X,\text{MgII}}$ that occurred in the grid. We also present the model responsible for this value of $\Gamma_{X,\text{MgII}}$. All values of $\Gamma_{X,\text{MgII}}^{\text{max}}$ should be treated as having an error of at least 0.3 dex. We find that these results are consistent with the predictions of MODEL 1 in Lopez et al. (1999) and are also consistent with their measured values.

4.1.3 A Search for Interlopers and Results

Having obtained estimates of the column density upper limits (Table 1), we can use the results of Fig. 3 to restrict the possible values for $\Delta\lambda$ for any of the species above. Fig. 3 shows the value of this test, since, given a value for $\Gamma_{X,\text{MgII}}$, we can place very stringent constraints on the allowed range in $\Delta\lambda$. Then, we search tabulated transitions for each species to see if any candidate interlopers exist.

Table 1 and the results expressed in Fig. 3 show that any interloper must have a wavelength differing by no more than $\sim 0.1 \text{\AA}$ to that of Mg II $\lambda 2796$. We searched published energy level tables (Moore 1971; the Vienna Atomic Line Database (VALD) – Piskunov et al. 1995 and Kupka et al. 1999) to find potential lines of those species shown in Table 1 which satisfy the above criteria. We searched only for E1 transitions as all other transitions are associated with a large factor of suppression. For example, E2 and M1 transition probabilities are suppressed by factors $\sim \alpha^{-2}$ and $\sim \alpha^{-2}(Z_n\alpha)^{-4}$ respectively (Z_n is the nuclear charge). Forbidden E1 transitions can also be considered since the

Table 1. Results of the CLOUDY photo-ionization equilibrium calculation showing the upper limit on $\Gamma_{X,\text{Mg II}} = \log_{10} \frac{N(X)}{N(\text{Mg II})}$. The model used is specified by the logarithmic parameters, U , $N(\text{H I})$, n_{H} and Z .

Ion	$\Gamma_{X,\text{Mg II}}^{\text{max}}$	U	$N(\text{H I})$	n_{H}	Z	Ion	$\Gamma_{X,\text{Mg II}}^{\text{max}}$	U	$N(\text{H I})$	n_{H}	Z
Fe I	-0.20	-4	19	-3	-2	Ni I	-2.39	-4	17	-3	-2
Fe II	0.62	-3	19	-3	0	Ni II	-0.79	-3	19	-3	0
Fe III	0.84	-3	17	-3	-2	Ni III	-1.07	-3	17	-3	-2
Fe IV	0.99	-3	17	-3	-2	Ni IV	-0.63	-3	17	0	-2
Fe V	0.42	-3	17	-3	-2	Ni V	-1.05	-3	17	-3	-2
Fe VI	0.11	-3	17	-3	-2	Ni VI	-0.62	-3	17	-3	-2
Fe VII	-0.71	-3	17	-3	-2	Ni VII	-0.92	-3	17	-3	-2
Fe VIII	-2.07	-3	17	-3	-2	Ni VIII	-1.79	-3	17	-3	-2
Mg I	-1.50	-4	19	-3	-2	Na I	-2.18	-4	17	-3	0
Mg III	1.16	-3	17	-3	-2	Na II	-0.80	-3	17	0	-2
Mg IV	0.19	-3	17	-3	-2	Na III	-0.23	-3	17	-3	-2
Mg V	-1.24	-3	17	-3	-2	Na IV	-0.74	-3	17	-3	-2
Mg VI	-2.20	-3	17	-3	-2	Na V	-1.82	-3	17	-3	-2
Al I	-2.02	-3	17	-3	-2	Si I	-1.53	-4	17	-3	0
Al II	-0.17	-3	17	-3	-2	Si II	0.62	-3	17	-3	0
Al III	-0.64	-3	17	0	0	Si III	1.09	-3	17	-3	-2
Al IV	-0.31	-3	17	0	0	Si IV	0.26	-3	17	0	-2
Al V	-1.37	-3	17	0	0	Si V	-0.62	-3	17	0	-2
Al VI	-2.28	-3	17	0	0	Si VI	-1.46	-3	17	0	-2
Ca I	-2.03	-4	17	-3	0	C I	-0.33	-4	17	-3	-2
Ca II	-1.32	-4	17	0	0	C II	1.53	-3	17	-3	-2
Ca III	-0.01	-3	17	-3	-2	C III	2.08	-3	17	-3	-2
Ca IV	-0.84	-3	17	-3	-2	C IV	0.85	-3	17	-3	-2
Ca V	-2.18	-3	17	-3	-2	C V	0.00	-3	17	-3	-2
N I	0.70	-4	19	0	0	O I	1.79	-3	19	-3	0
N II	1.01	-3	17	-3	-2	O II	1.88	-3	19	-3	0
N III	1.57	-3	17	-3	-2	O III	2.47	-3	19	-3	0
N IV	0.48	-3	17	-3	-2	O IV	1.13	-3	19	-3	0
N V	-1.03	-3	17	-3	-2	O V	-0.21	-3	19	-3	0
N VI	-1.89	-3	17	-3	-2	O VI	-1.70	-3	19	-3	0
Ne I	-0.22	-4	19	-3	0	Ar I	-1.24	-4	19	-3	-2
Ne II	0.57	-3	19	-3	0	Ar II	-0.53	-3	17	-3	-2
Ne III	1.68	-3	17	-3	-2	Ar III	0.01	-3	17	0	-2
Ne IV	0.68	-3	17	-3	-2	Ar IV	-0.89	-3	17	0	-2
Ne V	-0.70	-3	17	-3	-2	Ar V	-2.38	-3	17	-3	-2

oscillator strengths are typically $\sim 10Z_n^4\alpha^4$ times that of a normal E1 transition in a related or similar ion.

Oscillator strengths, f_X , are not generally available for the potentially interloping transitions, so we must adopt an upper limit by using other (stronger) transitions for the same multiplet (for which oscillator strengths are known).

Given upper limits on f_X and $\Gamma_{X,\text{Mg II}}$ and a value for $\Delta\lambda$, we can estimate $d\lambda$ and hence derive a conservative upper limit on the interloper's effect on $\Delta\alpha/\alpha$.

Although Fig. 3 relates specifically to Mg II $\lambda 2796$, similar simulations were carried out to search for interlopers near all other 'host' absorption lines (i.e. those in table 1 in M01a). The model parameters were also extended to DLAs (e.g. $19 < \log_{10} N(\text{H I}) < 22$).

We have *not been able to identify any candidate interlopers* satisfying all of the criteria above.

We note that CLOUDY only computes column densities for the most abundant species. However, it is possible that

other low abundance species could mimic a shift in α . Therefore, we searched for interloping lines (in Moore 1971 and VALD) of ionic species of elements such as Sc, Ti, V, Cr, Mn, Co and Zn and found only one possibility: a Cr II transition with $\lambda_0 = 2026.2686 \text{ \AA}$ which lies 0.13 \AA to the red of the Zn II $\lambda 2026$ 'host' line. This line has an oscillator strength of 0.047 according to VALD. We simulated its effect on $\Delta\alpha/\alpha$ for the high- z sample.

We obtained the largest value of $N(\text{Cr II})/N(\text{Zn II})$ directly from the observed QSO absorption line data. We then generated a synthetic, single velocity component spectrum containing Zn II $\lambda 2026$ and the Cr II interloper. We also generated several other lines seen in the high- z sample. We produce synthetic spectra with several different values of $\Delta\alpha/\alpha$ and then used VPFIT to measure $\Delta\alpha/\alpha$. The result was that the measured value of $\Delta\alpha/\alpha$ was always consistent with the nominal value, that is, we could detect no effect due to the interloping Cr II transition.

In summary, we have found no interloping species which could have caused a significant shift in $\Delta\alpha/\alpha$. We do note, however, that the ionic energy level data in Moore (1971) and VALD are incomplete for many highly ionized species and so we cannot rule out the possibility of blending with undiscovered transitions. Also, as noted previously, this analysis only takes into account blends with atomic, not molecular species. Firstly, typical oscillator strengths for molecular transitions are much smaller than for resonance atomic transitions. Also, the typical column densities of the low abundance elements in Table 1 suggest that very few molecules will exist in the QSO absorption clouds. Therefore, we consider the possible effect of any molecular blending to be negligible.

4.2 Line removal as a test for systematic blends

If a particular host transition (e.g. Mg II $\lambda 2796$) were systematically blended then removing that transition from the analysis in M01a and W01 should result in a different value of $\Delta\alpha/\alpha$. Line removal is also a rough test for isotopic ratio or hyperfine structure effects as introduced in Sections 2.3–2.5. We therefore remove a particular transition in an absorption complex only if doing so still allows us to obtain meaningful constraints on $\Delta\alpha/\alpha$. For example, we do not remove the Mg II $\lambda 2796$ line from a fit to a Mg II/Fe II system if the Mg II $\lambda 2803$ line is not present. We also removed entire species where possible. A small difficulty occurs with Cr II and Zn II $\lambda 2062$, whose profiles are sometimes blended together (i.e. when the velocity structure is broad). If the profiles were blended then we simply removed both transitions simultaneously, only removing them separately when the lines were completely separated. We obtain $\Delta\alpha/\alpha$ with the same procedure described in M01a.

Removing a transition from the fit may result in a slightly modified estimate for the velocity structure, revising the estimate for $\Delta\alpha/\alpha$ for that system. The question is, how robust is the estimate for $\Delta\alpha/\alpha$, averaged over the entire sample, to this line removal process?

We present our results in Fig. 4. For each transition removed, we compare the weighted mean of $\Delta\alpha/\alpha$ (and the associated 1σ error) before and after the line removal. It must be stressed that both the value and the errors are not independent and so interpreting Fig. 4 is difficult. However, it seems that there are no extreme deviations after line removal. Thus, we might conclude from such a diagram that systematic blending has not occurred and that we have no reason to suspect that one or more of the laboratory wavelengths is incorrect.

Concentrating on the heavier ions, we might also conclude that there is no effect on $\Delta\alpha/\alpha$ due to possible isotopic ratio or hyperfine structure effects. We cannot draw similar conclusions for Mg since we cannot remove all Mg lines simultaneously (this would prevent us from obtaining meaningful constraints on $\Delta\alpha/\alpha$ for the low- z sample). We also see that any lack of thermal equilibrium in the absorption clouds, leading to unequal population of the hyperfine levels of Al III (see Section 2.5), has had no significant effect on $\Delta\alpha/\alpha$. The large error bars on the Al III points reflect the fact that those lines are only present in 6 of our high- z systems.

Qualitatively, this line removal test suggests that there

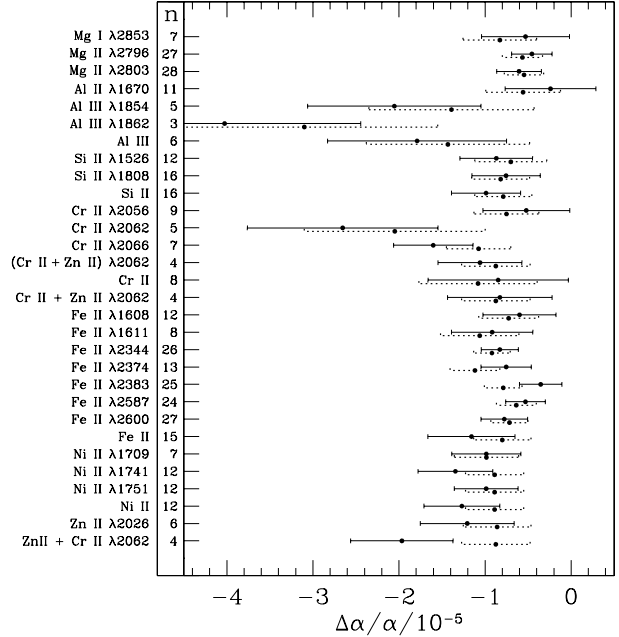


Figure 4. Comparison of the weighted mean of $\Delta\alpha/\alpha$ before (dotted error bar) and after (solid error bar) line removal. The transitions removed are listed on the left together with the number of systems, n , for which removal of that transition was possible. It is stressed that comparing the values and error bars before and after line removal is difficult since these quantities are not independent. Note that there may be some confusion due to the occasional blending of the Cr II and Zn II $\lambda 2062$ lines: ‘(Cr II + Zn II) $\lambda 2062$ ’ refers to cases where both transitions had to be removed simultaneously; ‘Cr II + Zn II $\lambda 2062$ ’ refers to cases when all Cr II transitions were removed along with the blended Zn II line; a similar definition applies to ‘Zn II + Cr II $\lambda 2062$ ’; ‘Cr II’ then refers only to the removal of all Cr II transitions in cases where there was no blending with the Zn II line. Only one similar case occurred for removal of all Zn II lines and so we do not present this result.

is no one single ‘host’ transition or species which is systematically blended and which has therefore affected our results in any significant way. The results also suggest that isotopic ratio or hyperfine structure effects have not significantly affected the heavier ions in our analysis. This point is more fully explored in Section 6 and 7.

5 DETAILED ANALYSIS: ATMOSPHERIC DISPERSION EFFECTS

The problems that arise due to atmospheric dispersion effects can be understood with reference to Fig. 5. If we observe a point source with the spectrograph slit at some angle θ to the vertical (as projected on the sky) then the object is dispersed with some component along the spectral direction of the slit. The optical design of the Keck/HIRES combination at the time at which a large fraction of our data was taken was such that $\theta = \xi$ for ξ the zenith angle of the object (Tom Bida, Steve Vogt, personal communication). As we noted in Section 2.12, this leads to two effects on the wavelength scale:

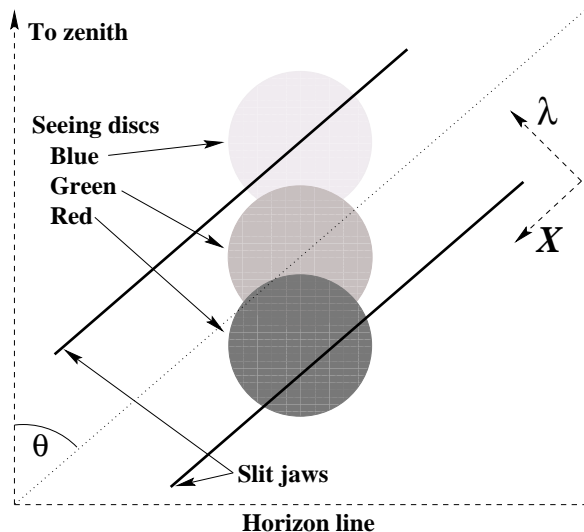


Figure 5. Schematic diagram showing the effects of atmospheric dispersion. The HIRES slit is projected onto the sky so that we see the seeing discs of blue, red and green light from a point source dispersed with some component along the spectral direction of the slit. The spectral direction is indicated by λ and the spatial direction by X . Note that the refraction is worse in the blue.

(i) The first effect is a stretching of the spectrum (relative to the ThAr calibration frames) due to the angular separation of different wavelengths entering the slit. Consider two wavelengths, λ_1 and λ_2 ($\lambda_2 > \lambda_1$), falling across the slit as in Fig. 5. If we were to measure the spectral separation between these two wavelengths on the CCD, $\Delta\lambda'$, we would find that

$$\Delta\lambda' \approx \lambda_2 - \lambda_1 + \frac{a\Delta\psi \sin\theta}{\delta}, \quad (6)$$

where a is the CCD pixel size in Ångströms, δ is the projected slit width in arc seconds per pixel (for HIRES, $\delta = 0''.287$ per pixel) and $\Delta\psi$ is the angular separation (in arc seconds) of λ_1 and λ_2 at the slit. $\Delta\psi$ is a function of the atmospheric conditions along the line of sight to the object and can be approximated using the refractive index of air at the observer and the zenith distance of the object (e.g. Filippenko 1982). Note that equation 6 assumes that the seeing profile is not truncated at the slit edges. If tracking errors or seeing effects cause truncation, equation 6 provides an upper limit to the measured $\Delta\lambda'$.

(ii) If truncation of the seeing profile does occur, it may be asymmetric (as the diagram illustrates). In the case of HIRES, the optical design is such that a blue spectral feature will have its red wing truncated and a red spectral feature will be truncated towards the blue. This is the case shown in Fig. 5. Thus, an asymmetry is introduced into the IP and this will be wavelength dependent. The extent of the asymmetry will depend on $\Delta\psi$ (which depends most strongly on ξ).

Note that when we centroid spectral features to find their separation, both effect (i) (shifting) and effect (ii) (instrumental profile (IP) distortion) effectively ‘stretch’ the spectrum. For the low- z sample, this should lead to systematically positive values of $\Delta\alpha/\alpha$. That is, atmospheric dispersion effects cannot explain the average negative value

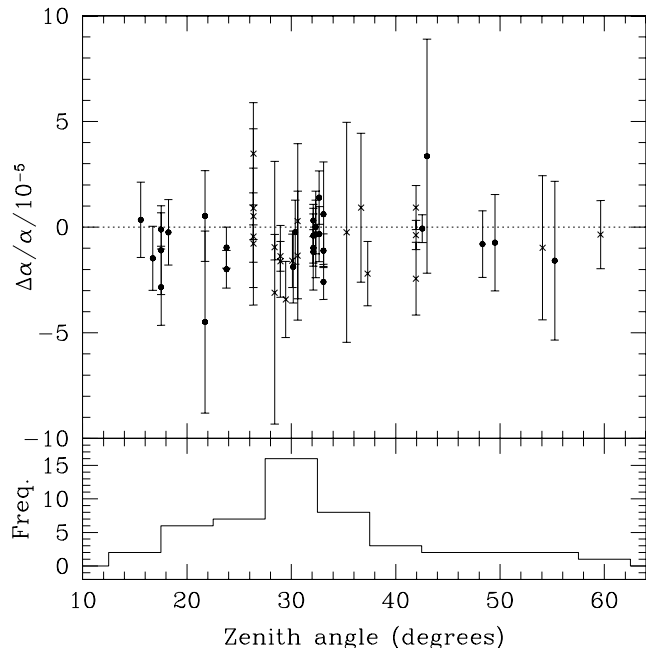


Figure 6. The lower panel shows the distribution of absorption systems over average zenith distance. The upper panel shows the QSO data as a function of zenith distance. We do not see any obvious correlation. When we remove points for which there should be no atmospheric dispersion effect, the Spearman rank correlation coefficient is 0.18 with an associated probability of 0.41. The coefficients for the low (filled circles) and high (crosses) redshift samples are 0.16 and -0.09 with probabilities 0.43 and 0.71 respectively.

of $\Delta\alpha/\alpha$ seen in the QSO data. Removing these effects from our data would make the results *more* significant. Although there is no obvious correlation between $\Delta\alpha/\alpha$ and ξ as would be expected in this scenario (see Fig. 6), the potential effect is quantified in our analysis below.

For all objects which were observed without the use of an image rotator, we have used the observational parameters reported in the image header files to find average values of ξ (see Fig. 6), temperature, pressure and relative humidity for each object. This allows us to correct for the stretching of the spectrum implied by equation 6. We have re-calculated $\Delta\alpha/\alpha$ in the same manner as described in M01a and we plot the results in Fig. 7. For several QSOs, only a single image header (i.e. for one of the QSO exposures out of a series) was available. In these cases we have added (in quadrature) an error of 0.9×10^{-5} . This is an average value determined by calculating $\Delta\alpha/\alpha$ for several values of the zenith distance for those objects concerned and corresponds to an uncertainty in the average ξ of about $\pm 20^\circ$.

We have also tested the effect of the IP distortions (effect (ii) above) on $\Delta\alpha/\alpha$. We generated high SNR, single component absorption spectra (with $\Delta\alpha/\alpha = 0$) for several redshifts. We included different combinations of transitions in the different spectra so as to make a representative estimate for both samples of QSO data (particularly the high- z sample which contains many combinations of different transitions). A wavelength dependent PSF was constructed using the following procedure. We assume that the

Table 2. Comparison of the weighted means, $\langle\Delta\alpha/\alpha\rangle_w$, with the results of M01a and W01, after correction for atmospheric dispersion effects.

Sample	$\langle\Delta\alpha/\alpha\rangle_w / 10^{-5}$	$\langle\Delta\alpha/\alpha\rangle_w^{\text{M01a}} / 10^{-5}$
Low- <i>z</i>	-1.52 ± 0.23	-0.70 ± 0.23
High- <i>z</i>	-0.79 ± 0.26	-0.76 ± 0.28
Total	-1.19 ± 0.17	-0.72 ± 0.18

seeing (taken as $0''.8$) and tracking error (taken as $0''.25$) generate Gaussian profiles across the slit and that a wavelength λ_0 falls at its centre. Other wavelengths are refracted to different parts of the slit depending on the zenith distance. To compute this, typical Keck atmospheric conditions (temperature, pressure, relative humidity) were used.

We truncate the profile by multiplying by a top-hat function (whose width is equal to that of the slit) and then convolve the result with a Gaussian IP of width $\sigma = 2.2 \text{ km s}^{-1}$ (Valenti et al. 1995). This final PSF is then convolved with the synthetic absorption spectra. The value of λ_0 is $\sim 5500 \text{ \AA}$ (i.e. the TV acquisition system is centred at about this wavelength). Using this value for λ_0 and $\xi = 45^\circ$ we find $\Delta\alpha/\alpha$ to be quite insensitive to the IP distortions, particularly in the high-*z* regime. The effect on $\Delta\alpha/\alpha$ may be as large as 0.05×10^{-5} for the low-*z* regime but round-off errors in VPFIT become important at this level of precision. To exaggerate the effect, we also chose extreme values of λ_0 to be 4000 and 7000 \AA . The effect on $\Delta\alpha/\alpha$ in these cases was still negligible in the high-*z* regime but increased to the level of $\Delta\alpha/\alpha \sim 0.12 \times 10^{-5}$ for the low-*z* spectra. This latter value corresponds to $\sim 1/6$ of the correction due to the shifting effect. The sign of the above corrections to $\Delta\alpha/\alpha$ are such that applying them to the QSO data make the observed average $\Delta\alpha/\alpha$ more negative.

In summary, we find $\Delta\alpha/\alpha$ to be most sensitive to the shifting effect described by equation 6 and reasonably insensitive to the IP distortion effect. Thus, we do not apply a correction for the latter in the results shown in Fig. 7. The results show the values of $\Delta\alpha/\alpha$ once the shifting effect has been removed from the data. As expected, we see a significant decrease in $\Delta\alpha/\alpha$ in the low-*z* sample. The high-*z* sample is insensitive to this systematic effect, as can be expected due to the many different transitions used with q_1 coefficients of different signs. We summarise the results in Table 2 and compare them with those found in M01a and W01. We stress that the corrections above (equation 6) are upper limits. Seeing and tracking errors will diminish the effects substantially.

6 DETAILED ANALYSIS: DIFFERENTIAL ISOTOPIC SATURATION

In this section we quantify the effect of differential isotopic saturation on our measured values of $\Delta\alpha/\alpha$. As discussed in Section 2.3, this comes about when the strongest isotopic component of an absorption line saturates. The weaker isotopic components may still be on the linear part of their curves of growth. Using a single weighted wavelength to represent the composite profile position (i.e. the profile cen-

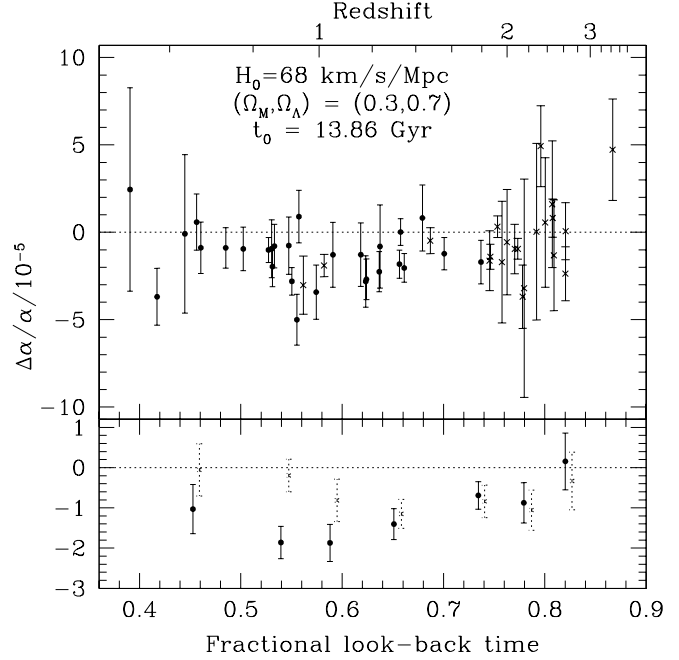


Figure 7. Results after removal of atmospheric dispersion effects. The top panel shows our raw results for $\Delta\alpha/\alpha$ as a function of look-back time in a flat, Λ cosmology. The redshift scale is also provided for comparison. The lower panel shows an arbitrary binning of the results which emphasizes the susceptibility of the low-*z* sample to this systematic error (the dotted lines are the results of M01a and W01, slightly shifted for clarity). Note, however, that the correction made here is an extreme and will be diminished by seeing and tracking effects.

teroid) can therefore, in principle, result in systematic errors in $\Delta\alpha/\alpha$.

The various isotopic abundances of concern are shown in Table 3. If only composite wavelengths were used then, if there exists a saturated dominant isotope in the QSO data, this may result in systematic errors in $\Delta\alpha/\alpha$. However, composite wavelengths were only used for the 4 heaviest atoms (i.e. Cr, Fe, Ni, Zn) and, of these, only some Fe transitions appear to be saturated in some of our QSO spectra. The Cr, Ni and Zn lines were always very weak (typically absorbing only $\sim 20\%$ of the continuum) and so using composite transition wavelengths is justified.

It is therefore left to quantify the effect of differential isotopic saturation for the Fe lines in our spectra. Ideally, if we knew the isotopic wavelength separations for the various Fe II transitions then we could do this by simply fitting our spectra with this structure to find $\Delta\alpha/\alpha$. The difference between the weighted mean $\Delta\alpha/\alpha$ and that found in M01a and W01 would indicate the size of the effect. In reality, we do not know the isotopic separations. We can, however, place an upper limit on this effect since we know (or can estimate) the isotopic separations of the Mg and Si anchor lines. If we fit our spectra with only the composite Mg and Si wavelengths then we will obtain maximal changes to $\Delta\alpha/\alpha$ since (i) these atoms have strong lines which saturate more often than the Fe II lines and (ii) they will have the largest isotopic separations (i.e. largest mass shift).

We have carried out the above re-calculation of $\Delta\alpha/\alpha$

Table 3. The percentage terrestrial abundances of the atoms used in our analysis (Rosman & Taylor 1998). The neutron number is defined relative to that of the isotope with the largest abundance and is denoted as ΔA (negative values representing lighter isotopes).

Atom	ΔA						
	-2	0	+1	+2	+3	+4	+6
Mg		78.99	10.00	11.01			
Al		100.0					
Si		92.23	4.68	3.09			
Cr	4.345	83.789	9.581	2.365			
Fe	5.845	91.754	2.119	0.282			
Ni		68.08		26.22	1.14	3.64	0.93
Zn		48.6		27.9	4.1	18.8	0.6

using the composite wavelengths for the Mg I, Mg II and Si II lines. In the low- z sample, the fact that the Mg lines have their weaker isotopes at shorter wavelengths means that $\Delta\alpha/\alpha$ should be systematically more negative if the composite wavelengths are used. The situation is again more complicated in the high- z sample. We find only very small differences between the results and those of M01a and W01, the weighted means for the low and high- z sample being $\Delta\alpha/\alpha = (-0.75 \pm 0.23) \times 10^{-5}$ and $\Delta\alpha/\alpha = (-0.74 \pm 0.28) \times 10^{-5}$ respectively (compared to $\Delta\alpha/\alpha = (-0.70 \pm 0.23) \times 10^{-5}$ and $\Delta\alpha/\alpha = (-0.76 \pm 0.28) \times 10^{-5}$ from M01a and W01).

Can we understand the magnitude of these corrections? Imagine a single velocity component and consider finding $\Delta\alpha/\alpha$ from, say, the Mg II $\lambda 2796$ and Fe II $\lambda 2344$ lines only. One might estimate the maximum effect of differential isotopic saturation by assuming that when all isotopes of Mg II are saturated, the line centroid would lie at the unweighted mean isotopic wavelength. This would result in a correction to $\Delta\alpha/\alpha$ of $\sim -1 \times 10^{-5}$ (i.e. the observed value would become negative when the correction is applied).

However, several factors will reduce this correction in reality. Firstly, once a line begins to saturate, then because the intrinsic line width (i.e. the b -parameter) is far greater than the isotopic separations, the weaker isotopes are swamped by the dominant one. This reduces the effect on $\Delta\alpha/\alpha$. Secondly, if the velocity structure is more complex (i.e. if it contains more than one velocity component) the unsaturated components, which do not suffer from the differential isotopic saturation problem, will provide much stronger constraints on $\Delta\alpha/\alpha$. Finally, as more unsaturated transitions (e.g. Fe II) are incorporated into the fit of a particular QSO absorption system, the effect is further reduced since some constraints on $\Delta\alpha/\alpha$ come from shifts between the Fe II lines.

It is therefore clear that differential saturation of the isotopic components of the various Fe II lines cannot have lead to any significant effect on $\Delta\alpha/\alpha$. Our results also indicate that the weighted mean $\Delta\alpha/\alpha$ for the high- z sample will not be very sensitive to errors in our estimate of the Si II isotopic separations.

Table 4. Wavelengths of the dominant isotopic components of the Mg and Si transitions. Those of Mg are derived from experimental data in Pickering et al. (1998) while those of Si are calculated in M01a on the basis of a scaling by the mass shift from the basic Mg isotopic structure.

Transition	m	ω_0	λ_0
Mg I $\lambda 2853$	24	35051.271	2852.9636
Mg II $\lambda 2803$	24	35669.286	2803.5324
Mg II $\lambda 2796$	24	35760.835	2796.3553
Si II $\lambda 1808$	28	55309.330	1808.0132
Si II $\lambda 1526$	28	65500.442	1526.7073

7 DETAILED ANALYSIS: ISOTOPIC ABUNDANCE VARIATION

The analysis we have carried out so far assumes terrestrial isotopic abundances. However, it is quite possible, even likely, that these high redshift gas clouds have rather different abundances. As we noted in Section 2.4, a substantial systematic shift in α might be mimicked and will be particularly pronounced in the low- z sample since the Mg isotopic separations are the largest. No observations of high redshift isotopic abundances have been made so we have no *a priori* information on the QSO absorption systems themselves. However, observations of Mg (Gay & Lambert 2000) and theoretical estimates for Si (Timmes & Clayton 1996) in stars clearly show a decrease in isotopic abundances with decreasing metallicity. For example, at relative metal abundances $[\text{Fe}/\text{H}] \sim -1$, $^{25}\text{Mg}/^{24}\text{Mg} \sim ^{26}\text{Mg}/^{24}\text{Mg} \approx 0.1$, i.e. about 20% below terrestrial values (see Table 3). Theoretical calculations (Timmes, Woosley & Weaver 1995) suggest even larger decreases.

Estimates have also been made of the metal abundances in a subset of the QSO absorption systems used in our analysis. The DLAs have a mean metallicity of $Z \sim -1.5$ (Prochaska & Wolfe 2000) and the Mg/Fe systems span the range $Z = -2.5$ to 0.0 (Churchill et al. 1999).

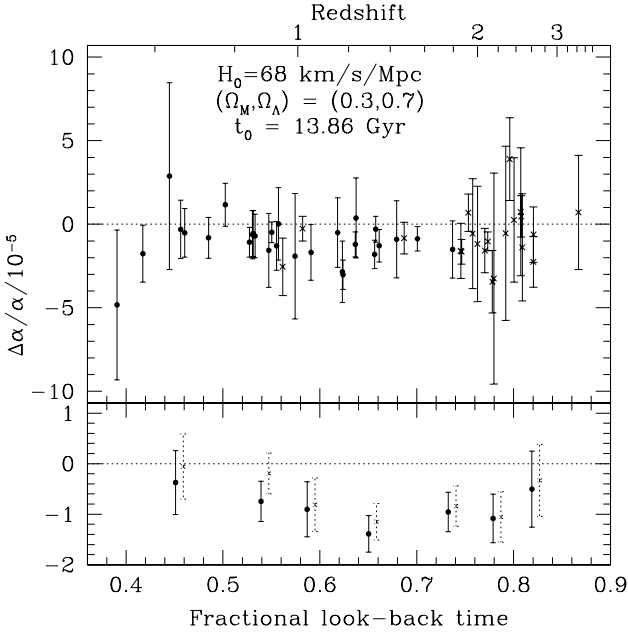
Therefore, we explored the effect of isotopic abundance evolution on $\Delta\alpha/\alpha$ for the entire range in isotopic abundance from zero to terrestrial values (i.e. in the case of Mg, the limiting case is $^{25}\text{Mg}/^{24}\text{Mg} = ^{26}\text{Mg}/^{24}\text{Mg} = 0$). This allows us to derive a secure upper limit on the magnitude of the effect on $\Delta\alpha/\alpha$.

We have re-computed $\Delta\alpha/\alpha$ for the entire sample after removing the following isotopes: ^{25}Mg , ^{26}Mg , ^{29}Si and ^{30}Si . The wavelengths for the dominant isotopic components, ^{24}Mg and ^{28}Si , for the various transitions of interest, are given in table 3 of M01a and are summarized in Table 4.

The results are presented in Table 5 and Fig. 8. These show, as expected, that the low- z sample is more sensitive to this systematic error than the high- z sample. We stress that the signs of the above corrections are such that applying them to the QSO data make the observed average $\Delta\alpha/\alpha$ *more negative*. Since we have no information on the isotopic separations for the other atoms of interest, we cannot perform a similar analysis for all species. However, the corrections due to variation in the isotopic abundances of Mg and Si should be dominant (as we discuss in Section 2.4) so

Table 5. Comparison of the weighted means, $\langle \Delta\alpha/\alpha \rangle_w$, with the results of M01a and W01, after maximal correction for possible variation in isotopic ratios

Sample	$\langle \Delta\alpha/\alpha \rangle_w / 10^{-5}$	$\langle \Delta\alpha/\alpha \rangle_w^{\text{M01a}} / 10^{-5}$
Low z	-1.01 ± 0.23	-0.70 ± 0.23
High z	-0.87 ± 0.26	-0.76 ± 0.28
Total	-0.96 ± 0.17	-0.72 ± 0.18

**Figure 8.** Results after removing the weaker isotopic components of Mg and Si. The upper panel shows our raw results and the lower panel shows an arbitrary binning which emphasizes the susceptibility of the low- z sample to this systematic error (the dotted lines are the results of M01a and W01, slightly shifted for clarity). Note, however, that the correction made here is extreme.

the corrections shown in Table 5 and Fig. 8 are conservative upper limits.

8 A GENERAL TEST FOR SYSTEMATIC ERRORS

Although we have already convincingly ruled out any significant wavelength-scale distortion using ThAr spectra (Section 3), the QSO and ThAr light does not follow precisely the same light path. Indeed, for these reasons we had to consider some of the previous effects such as atmospheric dispersion. Thus, it is conceivable that some residual long-scale wavelength distortion or other simple systematic error remains in the QSO spectra.

The dependence of $\Delta\alpha/\alpha$ on the q_1 coefficients is simple for the low- z sample but considerably more complicated for the high z sample. This can be seen by inspecting table 1 in M01a. If systematic errors are responsible for the non-zero $\Delta\alpha/\alpha$ we measure, it is therefore surprising that $\Delta\alpha/\alpha$ is so consistent between the 2 samples. *A priori*, it would be

Table 6. Results of a general test for systematic errors. We removed the three different *types* of transition from a sub-sample of the 21 high- z systems. The new $\Delta\alpha/\alpha$ is given for each case. These should be compared to the value obtained when only transitions with mediocre q_1 coefficients were removed. Note that neither the values or the 1σ errors are independent of each other.

Sub-sample removed	$\langle \Delta\alpha/\alpha \rangle_w / 10^{-5}$
None	-0.90 ± 0.34
Mediocre-shifters	-1.29 ± 0.39
Anchors	-1.46 ± 0.44
Negative-shifters	-1.34 ± 0.65
Positive-shifters	-1.39 ± 1.01

even more surprising if we were to take subsets of the QSO data, grouped according to the sign and magnitude of q_1 , and found a *consistent* value for $\Delta\alpha/\alpha$.

We apply this idea to the high- z sample only, since it contains transitions with a wide range of q_1 values. Of the 21 absorbers in this sample, we can find a subset of 13 systems that include at least one anchor line (transitions with small q_1), at least one positive-shifter ($q_1 \geq 700 \text{ cm}^{-1}$) and at least one negative-shifter ($q_1 \leq -700 \text{ cm}^{-1}$). If some kind of general long-scale distortion of the wavelength scale was present, we might expect to find a change of sign in the average $\Delta\alpha/\alpha$ when comparing, for example, the negative-shifters or positive-shifters against the anchors (see equation 1).

From these systems we remove all transitions with q_1 coefficients of ‘mediocre’ magnitude ($300 \leq |q_1| < 700 \text{ cm}^{-1}$) so as to clearly delineate the three types of transition (anchor, positive and negative-shifter). We then calculate $\Delta\alpha/\alpha$ for this sample. We then remove each type of transition separately and calculate $\Delta\alpha/\alpha$ again. There is a small complication due to the presence of the occasional blend between Cr II and Zn II $\lambda 2062$ since these lines shift in opposite directions. In cases where these two lines were blended together, we removed both of them from all fits since they are of different ‘type’ and cannot be removed individually.

We present our results in Table 6. Again, precise, quantitative comparison of the values of $\Delta\alpha/\alpha$ obtained with the various types of transitions removed is difficult since neither the values or the 1σ error are independent. Also, when we remove the positive shifters, the uncertainty in $\Delta\alpha/\alpha$ is quite large. However, we do not find any evidence to suggest that $\Delta\alpha/\alpha$ is somehow dependent on the sign of q_1 from this test. That is, the high- z results seem to be robust against the presence of simple systematic errors. Indeed, this is corroborated by the results of removing atmospheric dispersion effects (Table 2 and Fig. 7).

9 CONCLUSIONS

The most important conclusion of the work described here is that after a detailed search for instrumental and astrophysical effects, we have found no systematic effect which can easily mimic a negative $\Delta\alpha/\alpha$.

Of those effects we have identified and explored, two systematic effects have been found to be *potentially* significant: atmospheric dispersion and isotopic evolution. If we were

to remove these effects from the data, the resulting $\Delta\alpha/\alpha$ would actually be *more negative* than the uncorrected effect (see Figs. 7 and 8). These corrections are *not* applied to the data in M01a and W01 because (i) our estimates provide *upper limits* on the magnitude of the effects, and (ii) we prefer to be as conservative as possible as to the significance of the deviation of $\Delta\alpha/\alpha$ from zero.

Tighter constraints on α are possible for realistic SNR from current telescopes/spectrographs. The analyses above indicate that another order of magnitude precision can be gained using our methods before wavelength calibration and laboratory wavelength errors become significant. We hope that M01a, W01 and the present work encourage further well calibrated, higher SNR observations of QSOs and that an independent check on our results can be made.

ACKNOWLEDGMENTS

We are very grateful to Tom Bida and Steven Vogt who provided much detailed information about Keck/HIRES. We thank Ulf Griesmann, Svereric Johansson, Rainer Kling, Richard Learner, Ulf Litzén, Juliet Pickering and Anne Thorne for much detailed information about their laboratory wavelength measurements. We also acknowledge helpful discussions with Michael Bessel, Bob Carswell, Roberto De Propriis, Alberto Fernández-Soto, John Hearnshaw, Alexander Ivanchik, Jochen Liske and Geoff Marcy. We are grateful to the John Templeton Foundation for supporting this work. MTM and JKW are grateful for hospitality at the IoA Cambridge, where some of this work was carried out.

REFERENCES

Bahcall J. N., 1967, ApJ, 149, L7
 Bahcall J. N., Sargent W. L. W., Schmidt M., 1967, ApJ, 149, L11
 Barrow J. D., 1987, Phys. Rev. D, 35, 1805
 Bechtold J., Weymann R. J., Lin Z., Malkan M. A., 1987, ApJ, 315, 180
 Bergeron J., Stasińska G., 1986, A&A, 169, 1
 Bergeron J. et al., 1994, ApJ, 436, L33
 Churchill C. W., 1997, Ph.D. thesis, UC Santa Cruz
 Churchill C. W., Rigby J. R., Charlton J. C., Vogt S. S., 1999, ApJS, 120, 51
 Cowie L. L., Songaila A., 1995, ApJ, 453, 596
 Dirac P. A. M., 1937, Nat, 139, 323
 Drullinger R. E., Wineland D. J., Bergquist J. C., 1980, Appl. Phys., 22, 365
 Dzuba V. A., Flambaum V. V., Webb J. K., 1999a, Phys. Rev. Lett., 82, 888
 Dzuba V. A., Flambaum V. V., Webb J. K., 1999b, Phys. Rev. A., 59, 230
 Dzuba V. A., Flambaum V. V., Murphy M. T., Webb J. K., 2001, Phys. Rev. A, 63, 042509
 Edlén B., 1953, J. Opt. Soc. Am., 43, 339
 Edlén B., 1966, Metrologia, 2, 71
 Feretti L., Dallacasa D., Govoni F., Giovannini G., Taylor G. B., Klein U., 1999, A&A, 344, 472
 Ferland G. J., 1993, University of Kentucky Department of Physics and Astronomy Internal Report
 Filippenko A. V., 1982, PASP, 94, 715
 Forgács P., Horváth Z., 1979, General Relativity and Gravitation, 10, 931

Gay P. L., Lambert D. L., 2000, ApJ, 533, 260
 Griesmann U., Kling R., 2000, ApJ, 536, L113
 Hallstadius L., 1979, Z. Phys. A, 291, 1220
 Ivanchik A. V., Potekhin A. Y., Varshalovich D. A., 1999, A&A, 343, 439
 Kupka F., Piskunov N. E., Ryabchikova T. A., Stempels H. C., Weiss W. W., 1999, A&AS, 138, 119
 Li L. -X., Gott J. R. III, 1998, Phys. Rev. D, 58, 103513
 Lopez S., Reimers D., Rauch M., Sargent W. L. W., Smette A., 1999, ApJ, 513, 598
 Marciano W. J., 1984, Phys. Rev. Lett., 52, 489
 Milne E. A., 1935, Relativity, Gravitation and World Structure, Clarendon press, Oxford
 Milne E. A., 1937, Proc. Roy. Soc. A, 158, 324
 Moore C. E., 1971, Atomic Energy Levels As Derived From Analyses of Optical Spectra, Natl. Stand. Rel. Data Ser., Natl. Bur. Stand. (U.S.A.), Vol 1 and 2, U.S. Govt. Print Office, Washington, D.C., U.S.A.
 Morris S. L. et al., 1986, ApJ, 310, 40
 Murphy M. T., Webb J. K., Flambaum V. V., Dzuba V. A., Churchill C. W., Prochaska J. X., Barrow J. D., Wolfe A. M., 2001a, MNRAS, accepted (M01a) (astro-ph/0012419)
 Murphy M. T., Webb J. K., Flambaum V. V., Prochaska J. X., Wolfe A. M., 2001c, MNRAS, accepted (astro-ph/0012421)
 Nave G., Learner R. C. M., Thorne A. P., Harris C. J., 1991, J. Opt. Soc. Am. B, 8, 2028
 Norlén G., 1973, Phys. Src., 8, 249
 Palmer B. A., Engleman R. Jr., 1983, Atlas of the Thorium Spectrum, Los Alamos National Laboratory, Los Alamos, New Mexico
 Peck E. R., Reeder K., 1972, J. Opt. Soc. Am., 62, 958
 Pickering J. C., Thorne A. P., Webb J. K., 1998, MNRAS, 300, 131
 Pickering J. C., Thorne A. P., Murray J. E., Litzén U., Johansson S., Zilio V., Webb J. K., 2000, 319, 163
 Piskunov N. E., Kupka F., Ryabchikova T. A., Weiss W. W., Jeffery C. S., 1995, A&AS, 112, 525
 Prochaska J. X., 1999, ApJ, 511, L71
 Prochaska J. X., Wolfe A. M., 2000, ApJ, 533, L5
 Rosman K. J. R., Taylor P. D. P., 1998, Pure and Applied Chemistry, 70, 217
 Songaila A., Cowie L. L., Hogan C. J., Rugers M., 1994, Nat, 368, 599
 Steidel C. C., Sargent W. L. W., 1989, ApJ, 343, L33
 Timmes F. X., Clayton D. D., 1996, ApJ, 472, 723
 Timmes F. X., Woosley S. E., Weaver T. A., 1995, ApJS, 98, 617
 Valenti J. A., Butler R. P., Marcy G. W., 1995, PASP, 107, 966
 Varshalovich D. A., Potekhin A. Y., 1995, Space Sci. Rev., 74, 259
 Varshalovich D. A., Potekhin A. Y., Ivanchik A. V., 2000, in Dunford R. W., Gemmel D. S., Kanter E. P., Kraessig B., Southworth S. H., Young L., eds., AIP Conf. Proc. 506, X-ray and Inner-Shell Processes. Argonne National Laboratory, Argonne, Illinois, p. 503
 Weast R. C., 1979, Handbook of Chemistry and Physics (60th edition), CRC Press, Florida, p. E-387
 Webb J. K., Flambaum V. V., Churchill C. W., Drinkwater M. J., Barrow J. D., 1999, Phys. Rev. Lett., 82, 884 (W99)
 Webb J. K., Murphy M. T., Flambaum V. V., Dzuba V. A., Barrow J. D., Churchill C. W., Prochaska J. X., Wolfe A. M., 2001, Phys. Rev. Lett., accepted (W01) (astro-ph/0012539)
 Whaling W., Anderson W. H. C., Carle M. T., Brault J. W., Zarem H. A., 1995, J. Quant. Spectrosc. Radiat. Transfer, 53, 1